ENN Encyclopedia of Nanoscience and Nanotechnology
www.aspbs.com/enn

Micro and Nanocantilever Sensors

P. G. Datskos, T. Thundat, Nickolay V. Lavrik

Oak Ridge National Laboratory, Oak Ridge, Tennesee, USA

CONTENTS

1. Introduction
2. Cantilever Sensors
3. Cantilever Sensor Characteristics
4. Nanocantilevers
5. Future Outlook
Glossary
References

1. INTRODUCTION

Cantilever structures are the simplest micro-electro-mechanical systems (MEMS) that can be easily micromachined and mass produced. The ability to detect extremely small displacements make the cantilever beams an ideal device for detection of extremely small forces and stresses. Here we assume that the displacement is directly proportional to the force acting on the cantilever beam. In general, small cantilever beams execute thermal motion (Brownian motion) with amplitudes proportional to the square root of the thermal energy. Measuring the thermal motion amplitude as a function of frequency enables the determination of resonance frequency of the cantilever beam.

Adsorption of molecules on the surface of a cantilever changes the total mass and, consequently, the resonance frequency of the cantilever. The resonance frequency of a microcantilever varies sensitively as a function of mass loading due to molecular adsorption [1–7]. The resonance frequency of a cantilever beam depends on its dimensions, elastic modulus, and density. By changing the dimensions, the resonance frequency can be varied from hundreds of Hz to hundreds of MHz. In fact, depending on the material when the cantilever is of nanoscale dimensions, GHz frequencies can be expected. For a given thickness, shorter cantilevers have higher resonance frequency than longer cantilevers. For a cantilever of given mass, higher resonance frequency implies a larger spring constant. The effect of damping due to medium density is higher for higher resonance frequencies. Although many cantilever sensors take advantage of adsorption-induced bending as the transduction method, an approach based on resonance frequency shifts can potentially provide ultimate sensitivity for detection of a single molecule.

If molecular adsorption is confined to one side of the cantilever, the cantilever undergoes bending due to adsorption-induced variation in surface stress [1–4, 8]. Molecular adsorption onto cantilevers that have two chemically different surfaces results in a differential stress between the top and bottom surfaces of the cantilever. The differential stress produces microcantilever bending. Generally, adsorption decreases the surface energy. For small bending of a cantilever, the surface stress variation can be equated to the variation of surface-free energy. The extent of cantilever bending is directly proportional to the surface-free energy variation due to molecular adsorption. Therefore, the cantilever bending due to molecular adsorption depends on the change in free energy per adsorbate and the total number of molecules taking part in the adsorption process. The extent of bending depends on the spring constant of the cantilever. In fact, for smaller spring constant cantilevers, the deflection of the cantilever will be larger.

2. CANTILEVER SENSORS

The typical thickness of a commonly used microcantilever is approximately 1μm. The length of the cantilever can vary from tens of μm to a few hundred μm. The spring constants of the cantilevers are typically in the range of 0.1 N/m. Microcantilevers are usually fabricated from silicon using standard photolithographic and etching techniques. A silicon nitride or a silicon dioxide film is deposited on a single-crystal silicon wafer by a low-pressure chemical vapor deposition (LPCVD) process. By varying the conditions of LPCVD, efforts are made to reduce the stress and stress gradient in the film so that the cantilevers are flat and unbent when fabricated. The nitride or oxide films are then patterned by photolithography, and the cantilever shapes are defined on the top surface and the etch masks on the bottom surface. The silicon substrate is then etched away to produce free-standing cantilevers. A metal layer such as gold can be coated onto either side of the cantilever, either to provide a surface for chemical modification through alkanethiol

ISBN: 1-58883-001-2/$35.00
Copyright © 2004 by American Scientific Publishers
All rights of reproduction in any form reserved.

Encyclopedia of Nanoscience and Nanotechnology
Edited by H. S. Nalwa
Volume X: Pages (1–10)

linkers or to make the surface nonreactive for silane-amino linkages of molecules to the oxide surface.

Adsorption-induced cantilever deflection and resonance frequency variation can form the basis of a universal platform for real-time, *in-situ* measurement of physical, chemical, and biochemical properties. A plethora of physical, chemical, and biological sensors, based on the micromachined cantilever platform, have already been demonstrated [1–4, 8–18]. Because cantilever bending and resonance frequency can be measured simultaneously, sensors can be based on adsorption-induced resonance frequency shifts and/or cantilever bending. The resonance frequency shifts and bending of a cantilever can be measured with very high precision using different readout techniques [19], such as optical beam deflection, variations in piezoresistivity, capacitance, and piezoelectric properties.

2.1. Thermal Motions of a Cantilever

The resonance frequency of a cantilever, f, is given by

$$f = \frac{1}{2\pi}\sqrt{\frac{K}{m^*}} \tag{1}$$

where K is the spring constant and m is the effective mass of the cantilever. The effective mass can be related to the mass of the beam, m, through the relation $m^* = nm$, where n is a unitless geometric parameter. For a rectangular cantilever, n has a typical value of 0.24 [20]. For a rectangular cantilever sensor, the spring constant for vertical deflection is given by [19]:

$$K = \frac{Ewt^3}{4L^3} \tag{2}$$

where E is the modulus of elasticity for the composing material and w, t, L are the width, thickness, and length of the beam, respectively. From eq. (1), it is clear that longer cantilevers have smaller spring constants. Therefore, longer cantilevers are more sensitive for measuring surface stresses. However, increasing the length also increases the thermal vibrational noise of the cantilever [19], which from statistical physics, is

$$\delta_n = \sqrt{\frac{2k_BTB}{\pi k f_0 Q}} \tag{3}$$

Here, k_B is the Boltzmann constant (1.38×10^{-23} J/K), T is the absolute temperature (300 K at room temperature), B is the bandwidth of measurement (typically about 1000 Hz for dc measurement), f_0 is the resonant frequency of the cantilever, and Q is the quality factor of the resonance which is related to damping.

It is clear from eq. (3) that lower spring stiffness produces higher thermal noise. It is important to note that the resonance frequency f_0 may undergo noticeable fluctuations, Δf_0, due to exchange between the mechanical and thermal energy of the cantilever [21]:

$$f_0 = \frac{1}{A}\sqrt{\frac{2\pi k_BTB}{KQf_0}} \tag{4}$$

where T is the absolute temperature, Q is the quality factor of the cantilever oscillator, and B is the measurements bandwidth. Although eq. (4) predicts increased absolute fluctuations of the resonance frequency, f_0, as the resonance frequency f_0 increases, relative frequency instability, $\Delta f_0/f_0$, decreases in the case of higher frequency oscillators

$$\frac{\Delta f_0}{f_0} = \frac{1}{A}\sqrt{\frac{2\pi k_BTB}{KQf_0}} \tag{5}$$

2.2. *Q*-Factor

The quality factor, or Q-factor, of a resonator is a measure of the spread of the resonance peak, Δf_0, and is thus related to energy loss due to damping ($Q = \Delta f_0/f_0$). The lower the Q-factor, the more damped the oscillator. The Q-factor depends on parameters such as cantilever material, geometrical shape, and the viscosity of the medium. Typically, the Q-factor of a rectangular silicon cantilever in air is approximately 30. However, in solution, the Q-factor decreases by a factor of 10. Therefore, measurements of adsorbed mass based on resonance frequency variation suffer from low resolution in liquid environment. Recently, it has been shown that the effective Q-factor can be increased by two to three orders of magnitude by a feedback mechanism [22]. In the feedback technique, the position sensitive detector (PSD) signal is fed back to a piezoelectric element that oscillates the cantilever into resonance. This technique also works with thermal motion of the cantilever.

2.3. Signal Transduction

For a cantilever with a dimension in tens of microns, the bending and resonance frequency shifts are measured with high precision using optical reflection, piezoresistive, capacitance, and piezoelectric methods. One great advantage of the cantilever technique is that both bending and resonance frequency can be measured in a single measurement. Moreover, other resonance parameters such as phase, amplitude, and Q-factor can be determined if a frequency spectrum is obtained. All the signal transduction methods are compatible with array format.

2.3.1. Optical Beam Deflection

The simplest way of measuring cantilever deflection is by optical beam deflection [19, 23]. In optical beam deflection technique, a laser diode is focused at the free end of the cantilever. The reflected beam is monitored using a position-sensitive detector. Displacement of the order of 0.1 nm can be measured using optical beam deflection. Optical beam deflection has many advantages such as being compatible with use under liquid and lack of electrical contact to the cantilever beam. Optical beam deflection technique cannot be used when refractive index of the medium changes during exposure to analytes.

2.3.2. Piezoresistance Method

Piezoresistivity is the variation of bulk resistivity with applied stress. Doped silicon exhibits a strong piezoresistive effect [24–27]. The resistance of a doped region on a cantilever

can change reliably when the cantilever is stressed with deflection. This deflection can be caused by changes in adsorption-induced stress or by externally applied stress, such as thermal stress. The variation in cantilever resistance can be measured using an external, dc-biased, Wheatstone bridge. Typical resistance of a silicon microcantilever with a doped boron channel is a few kΩ. If the resistances in the Wheatstone bridge is assumed to have identical values, R, and an applied voltage V, the differential voltage across the bridge can be expressed as $\Delta V = V\Delta R/(4R)$. If the cantilever is designed to have two identical legs, the current can flow in and out of the cantilever through boron channels. Metallic interconnects can be made to the boron channels at the base of the cantilever for application of external power. The disadvantage of the piezoresistive technique is that it requires passing a current through the cantilever for displacement measurements. This results in electronic noises and thermal drift in cantilever deflection. In addition, the cantilever beam is at a higher temperature due to resistive losses in the cantilever. Since the cantilever temperature is above ambient temperature, any changes in flow rate or thermal conductivity of the ambient can cause parasitic cantilever deflection.

2.3.3. Piezoelectric Method

Piezoelectric technique utilizes overlayers that are piezoelectric on the cantilever. Thin layers of piezoelectric materials such as ZnO induces transient charge due to cantilever movement [28–30]. One disadvantage of the piezoelectric technique is that it requires electrodes to the piezoelectric film. In addition, for measurable piezoelectric signals, the film needs to be thicker. Piezoelectric technique is difficult to use when static cantilever deflection measurements are needed. Piezoelectric cantilevers are ideal for resonance, frequency-based approaches.

2.3.4. Capacitance Method

The capacitance variation technique of measuring cantilever deflection makes use of the variation in capacitance between cantilever and a fixed substrate [17, 31]. The capacitance varies sensitively as a function of cantilever bending. Capacitance technique, however, is not suitable for liquid environments. Also, variation in the dielectric constant of ambient can contribute to cantilever bending signal.

2.4. Advantages of Cantilever Sensors

One great advantage of the cantilever-based sensors is that four resonance response parameters (resonance frequency, phase, amplitude, and Q-factor) can be measured simultaneously. Another compelling feature of microcantilever sensors is that they can be operated in air, vacuum, or liquid. The damping effect in a liquid medium, however, reduces the resonance response of a microcantilever. In most liquids, the observed resonance response is approximately an order of magnitude smaller than that in air. The bending response, however, remains unaffected by the presence of a liquid medium. Therefore, the feasibility of operating a microcantilever in a solution with high sensitivity makes the microcantilever an ideal choice for biochemical sensors. Therefore, microfabricated cantilevers can provide the basis for a universal platform for real-time, *in-situ* measurement, and determination of physical, chemical, and biochemical properties. Cantilever sensors offer improved dynamic response, greatly reduced size and high precision, and increased reliability compared to conventional sensors. They are the simplest micromechanical systems that can be mass-produced with conventional micromachining techniques. They can be fabricated into multielement sensor arrays and fully integrated with on-chip electronic circuitry. Because the thermal mass of microcantilevers is extremely small, they can be heated and cooled with a thermal time-constant of less than a millisecond. This is advantageous for rapid reversal of molecular absorption processes and regeneration purposes. Therefore, the micromechanical platform offers an unparalleled opportunity for the development and mass production of extremely sensitive, low-cost sensors for real-time *in-situ* sensing of many chemical and biological species. Therefore, cantilever sensors with extremely high sensitivity can be fabricated by simply reducing the cantilever dimensions. These cantilevers with reduced sizes belong to a class known as nano-electro-mechanical systems (NEMS). Reducing the dimension increases energy efficiency, time response, and sensitivity. However, decreasing the cantilever size results in increased difficulties in fabrication as well as monitoring cantilever response.

3. CANTILEVER SENSOR CHARACTERISTICS

The most important aspect of any sensor is its sensitivity, selectivity, and the ability for regeneration. Since cantilever-based sensors are extremely sensitive displacement sensors, they do not offer any intrinsic chemical selectivity. For cantilever-based sensors, the chemical selectivity is obtained by utilizing chemically selective layers such as polymeric films, self-assembled monolayers, or antibody-antigen layers. Regeneration of the sensor originates from thermodynamics. If the analyte-substrate interaction energy is large, the sensor may not regenerate at room temperature.

As pointed out earlier, the cantilever sensor can be operated in two modes: resonance frequency variation and adsorption-induced cantilever bending approach. The sensitivity of the cantilever bending increases as the spring constant of the cantilever is reduced. Therefore, longer cantilevers with very small spring constants are attractive for use with the adsorption-bending method. However, thermal motion of the cantilever severely limits the extent by which the spring constant of the cantilever can be reduced. On the other hand, the sensitivity of resonance frequency shifts based-approach increases as a function of frequency of operation. Therefore, shorter, higher frequency cantilevers are more suitable for increasing the detection limit when utilizing an approach that takes advantage of frequency shifts.

3.1. Sensitivity of Resonance Frequency-Based Approach

Assuming the contribution from variation in spring constant is small, a mass dependence of the fundamental frequency can be written by combining eqs. (1) and (2) as

$$f = \frac{1}{2\pi}\sqrt{\frac{K}{m^*}} = \frac{t}{2\pi(0.98)L^2}\sqrt{\frac{E}{\rho}} \tag{6}$$

where ρ is the density of the cantilever material. The mass of the adsorbed material can be determined from the initial and final resonance frequency and the initial mass of the cantilever as

$$\frac{(f_1^2 - f_2^2)}{f_1^2} = \frac{\delta m}{m} \tag{7}$$

where f_1 and f_2 are the initial and final frequency, respectively, and δm and m are adsorbed mass and initial mass of the cantilever, respectively. If the adsorption is uniform on the cantilever surface, eq. (7) needs to be modified appropriately in order to take into account the effective mass of the cantilever.

The mass sensitivity of a cantilever sensor can be written as

$$S_m = \lim_{\Delta m \to 0} \frac{1}{f}\frac{\Delta f}{\Delta m} = \frac{1}{f_0}\frac{df}{dm} \tag{8}$$

where Δm and dm are normalized to the active sensor area of the device ($\Delta m = \delta m/A$, where A is the area of the cantilever). As can be seen from the expression in eq. (8), the sensitivity is the fractional change of the resonant frequency of the structure with addition of mass to the sensor. When applying this definition to the case of the cantilever sensor, the sensitivity can be expressed as

$$S_m = \frac{1}{\rho t} \tag{9}$$

where ρ and t are the density and the thickness of the cantilever, respectively. If mass is added uniformly on a cantilever, its resonance frequency decreases as a function of adsorbed mass. Note that the sensitivity of a cantilever sensor depends only on its thickness and material density.

Another characterization parameter of a cantilever sensor is its minimum detection mass density. The minimum detectable mass density can be obtained by rearranging eqs. (6) and (7) as

$$\Delta m_{\min} = \frac{1}{S_m}\frac{\Delta f_{\min}}{f} \tag{10}$$

where $\Delta m_{\min}$ is the minimum detectable mass density and $\Delta f_{\min}$ is the minimum detectable frequency shift. Typically, minimum detectable mass density values are experimentally quoted results due to specifics of the sensor as well as the frequency detection limitations determining $\Delta f_{\min}$. Therefore, by changing the physical dimension of a cantilever, one can increase its detection limits by many orders of magnitude.

The absolute limit of minimum detection can be derived by combining eqs. 4 and 5. The smallest (noise limited) detectable change in the resonator mass per unit area can be expressed as

$$\Delta m_{\min} = 8\sqrt{\frac{2\pi^5 K k_B T B}{f_0^5 Q}} \tag{11}$$

3.2. Sensitivity of Adsorption-Induced Cantilever Deflection Approach

As mentioned earlier, thin microcantilevers also undergo bending due to mechanical forces generated by molecular adsorption, one of the most overlooked yet fascinating aspects of adsorption. These adsorption-induced forces can be easily detected on so-called "real surfaces" such as the surface of a microcantilever operated in air or under liquid. Adsorption-induced forces are applicable only for monolayer films and should not be confused with bending due to dimensional changes such as the swelling of thicker polymer films on cantilevers. Adsorption-induced stress sensors have sensitivities three orders of magnitude higher than frequency variation (for resonance frequencies in the range of tens of kHz) based on adsorbed mass. In addition, adsorption-induced cantilever bending is ideal for liquid-based applications.

Using Stoney's formula [32], we can express the radius of curvature of cantilever bending due to adsorption as to adsorption as

$$\frac{1}{R} = 6\frac{(1-\upsilon)}{Et^2}\delta\sigma \tag{12}$$

where R is the cantilever's radius of curvature; υ and E are Poisson's ratio and Young's modulus for the substrate, respectively; t is the thickness of the cantilever; and $\delta\sigma$ is the differential surface stress. The differential surface stress is the difference between the surface stress of the top and bottom surfaces of the cantilever beam in units of N/m or J/m^2. Typically, the microcantilevers have spring constants in the range of 0.1 N/m. Using geometry, a relationship between the cantilever displacement and the differential surface stress can be expressed as

$$z = \frac{3L^2(1-\upsilon)}{Et^2}\sigma \tag{13}$$

where L is the length and h is the deflection. Equation 13 shows a linear relation between cantilever bending and differential surface stress. Therefore, any variation in the differential surface stress can result in cantilever bending. When confined to one surface, molecular adsorption on a thin cantilever can cause large changes in surface stress. Surface stress, σ, and surface free energy, γ, can be related using the Shuttleworth eqn. [33]

$$\sigma = \gamma + \left(\frac{\partial\gamma}{\partial\varepsilon}\right) \tag{14}$$

where σ is the surface stress. The surface strain $\partial\varepsilon$ is defined as a ratio of change in surface area, $\partial\varepsilon = \delta A/A$. Since the bending of the cantilever is very small compared to the

length of the cantilever, the strain contribution is only in the ppm (10^{-6}) range while the surface free-energy changes are in the 10^{-3} range. Therefore, one can easily neglect the contribution from surface strain effects and equate the free-energy change to surface stress variation.

4. NANOCANTILEVERS

Microcantilevers designed for scanning probe microscopy (SPM) applications have a resonance frequency in the 10–300 kHz range depending on the spring constant. The cantilevers used in SPM typically have dimensions in the 100 microns range and are fabricated by micromachining. These cantilevers demonstrate to be excellent sensors based on resonance frequency variation or cantilever bending. For a microcantilever, the sensitivity of mass detection increases with higher spring constant while bending signal sensitivity increases with lower spring constant. It is demonstrated that a mass resolution of approximately 1 pg can be achieved for a 200-micron-long cantilever with a resonance frequency of 25 kHz. The mass sensitivity of a microcantilever sensor can be greatly increased by decreasing its dimensions [34–36]. It is conceivable that reducing the dimensions of a cantilever sensor can lead to detection of individual binding events of molecular adsorption on a cantilever.

The cantilevers with reduced dimensions are called nanocantilevers. Nanocantilevers typically have a length of approximately 1 μm. The thickness and width of a nanocantilever are adjusted such that the cantilever is free from size-induced deformations. One advantage of decreasing the length of the cantilever is that its resonance frequency can be increased into MHz. Higher resonance frequency implies higher spring constant. Since these cantilevers have higher spring constants, they are not suitable for detecting adsorption-induced cantilever bending. Therefore, the nanocantilevers are more suited for a resonance frequency variation-based sensing approach than a bending-based method. However, it is possible to design a nanocantilever with a spring constant around 1 N/m by adjusting the length, width, and thickness. Davis et al. calculate a resonance frequency of 179.9 MHz for a cantilever of 2.82 microns long with a spring constant of 1 N/m [37].

In the case of resonating cantilevers scaled down to the nanosizes, further dramatic increases in their sensitivity to chemical or biological stimuli are expected providing an opportunity to achieve ultra-high mass sensitivity, ultimately, approaching detection to the single molecule level [38]. The minimum detectable mass strongly depends on K and Q and is given by [38]:

$$\Delta m_{\min} = \frac{8G}{\langle z^2 \rangle^{1/2}} \frac{m_0^{5/4}}{K^{3/4}} \sqrt{\frac{k_B T B}{Q}} \tag{15}$$

where G is a geometrical factor of the cantilever, k_B is the Boltzmann constant, T is the temperature of the cantilever, B is the bandwidth of the measurement, m_0 is the initial cantilever mass, and $\langle z^2 \rangle^{1/2}$ is the root mean-square amplitude of the cantilever motion. Therefore, both increased stiffness and the mass of the externally actuated resonator can influence the mass sensitivity. From eq. (15), however, it is clear that there is a connection between effects of the resonator stiffness and mass and the Q-factor. Obviously, accurate predictions of the mechanical quality factors are needed in order for eq. (15) to accurately predict the mass limit for nanocantilevers.

In addition to analytical implications, single-molecule detection is also very important for many fundamental areas of physics, chemistry, and biology. Nanomechanical structures capable of detecting single-molecule interactions have the potential for providing real-time information that cannot be obtained using the currently available methods.

In addition to sensing applications, nanocantilevers may also find applications in imaging such as scanning probe microscopy where fast imaging is needed. In this case, the cantilever beam is used for detecting force gradients that exists on the sample surface. The detectable force resolution of the cantilever is given by $(Kk_B/f_0Q)^{1/2}$. By varying the dimension, the cantilevers can be made sensitive to detect force gradients or to increase the resonance frequency and thus the scanning speed. It is possible to increase the resonance frequency without significantly changing the spring constant by optimizing the dimensions. In other applications, smaller dimensions of the nanocantilever will tend to increase the spatial resolution in techniques for *in-situ* mapping of molecular beams [39].

It should be pointed out that many of the signal transduction techniques for cantilever deflection measurements discussed in Section 2, such as optical beam deflection, are not suitable when cantilever length is reduced below 20 μm. Davis et al. demonstrated a cantilever signal detection based on capacitive readout [37]. In this sensor, the nanocantilever was excited into resonance electrostatically by means of a lateral electrode. The detection of oscillation amplitude of the cantilever was achieved by measuring displacement current in the capacitor formed by the cantilever and the driver electrode. The length of the cantilever was 50 microns. Kawakatsu et al. [40] fabricated nanocantilevers (nanometric oscillators) using silicon-etching processes. The cantilever was a nanometric tip with an elastic neck where the tip was fabricated by anisotropic etching of silicon by KOH. Burger et al. demonstrated nanocantilever fabrication based on focused ion beam (FIB) patterning/milling and KOH etching [41]. These nanocantilevers were 30 nm thin and 100 nm wide with lengths ranging from 0.5–2 microns.

As mentioned earlier, signal transduction is a formidable challenge for nanocantilevers. This challenge, however, can be overcome by utilizing a signal transduction method based on electron transfer that is ideally suited for detection of nanocantilever motion. As an electrically floating cantilever vibrates between two biased electrodes, a current flows through the system due to charge transfer between the electrodes through the floating cantilever. The basic concept of charge transport is similar to a electrostatic charge shuttle demonstrated by Tuominen et al. [42].

4.1. Nanocantilever Fabrication

Single crystal and polycrystalline cantilever structures routinely fabricated by a number of conventional processes of wet or dry etching. The dry etching process involves etching in inductively coupled plasma systems. Cantilevers

can also be fabricated using photo-electrochemical etching using etch stops. These conventional techniques of fabricating cantilevers using micromachining techniques are ideal for cantilevers that are tens of μm in size. However, fabrication of cantilevers with dimensions of only a few μm or smaller is still a formidable task. There exist a number of ways by which nanocantilevers can be fabricated, such as FIB or a combination of FIB and etching. Abadal et al. [7] have demonstrated two different types of fabrication techniques—one based on a combination of laser and atomic force microscopy (AFM) lithography and a second one based on electron beam lithography (EBL) [43]. In AFM lithography, a cantilever is fabricated on an Al-coated SiO_2 surface by oxidation. Electron beam lithography utilized a lift-off defined chrome layer as a mask for SF_6-based reactive ion etching. Cantilevers with a width of 100 nm and with varied lengths between 10 μm to 40 μm have been fabricated. However, none of these techniques are compatible with mass production.

Nanofabrication using a FIB is more compatible with mass production [38, 44]. In the FIB technique, a focused Ga ion beam with energy in tens of KeV is used to physically cut out cantilevers from thin silicon membranes. We used this technique where the starting surfaces for fabricating cantilevers were single-crystal Si membranes having an initial thickness of 10 μm. Prior to cantilever fabrication, the FIB was used to reduce the thickness of the Si membrane down to a few micrometers.

Cantilevers with dimensions 0.8 to 2 μm in length, 50 nm to 500 nm in width, and 25 to 100 nm in thickness, have been fabricated using FIB. The calculated resonance frequency of a rectangular Si cantilever with these dimensions is 265 MHz. The FIB technique can be used to nanofabricate devices from different materials and not limited to only Si.

A different approach that involves a combination of a focused ion beam and anisotropic wet etching can also be used for single-crystal substrates [41, 43, 45]. In this case, the focused Ga ion beam is used to dope specific parts of the target, single-crystal surface. Selective Ga ion implantation and subsequent milling by FIB exposure followed by wet chemical etching can be used to fabricate nanomechanical structures in single-crystal Si. Nanobridges and nanocantilevers with around 30 nm thickness can be made by controlled selective underetching between unexposed and exposed areas. In Figure 1, we show an example of nanomechanical bridges fabricated using the FIB doping technique. The patterned Ga ion implantation was performed on a (100) Si wafer and the effective doping depth was estimated to be around 70 nm. Anisotropic etching was performed on the implanted samples at 83 °C using KOH.

4.2. Nanocantilever Measurements

As indicated earlier, optical detection of cantilever motion of nanocantilevers and nanocantilever arrays at their resonance frequency is extremely difficult due to the reduced reflection (scattered) signal from the cantilever surface. Other techniques, such as piezoelectric and piezoresistive techniques, are harder to implement at nanoscale. Davis et al. [37] demonstrated capacitive-based signal transduction for 30–50 μm long cantilevers. However, as the cantilever dimensions are reduced, the capacitance signal will become comparable to parasitic capacitance from lead wires and bonding pads. Direct integration of CMOS circuitry on the cantilever chip can reduce the parasitic capacitance. Other techniques, such as electron tunneling and electron shuttling, can be used as signal transduction techniques for nanocantilevers since the amplitude of vibration is within nanometer range. In an electron tunneling device, the electrons tunnel between two surfaces maintained at a potential difference and separated by a few nanometers. In electron shuttling, the cantilever is vibrated between two surfaces maintained at a potential difference. Both electron tunneling and shuttling mechanisms can be used with ease when nanocantilevers are involved.

In electron shuttling signal transduction, a nanocantilever is nanofabricated between two fixed electrodes using FIB. The cantilever and the associated electrode system were fabricated monolithically using an FIB from a silicon membrane. A scanning ion micrograph of the monolithic

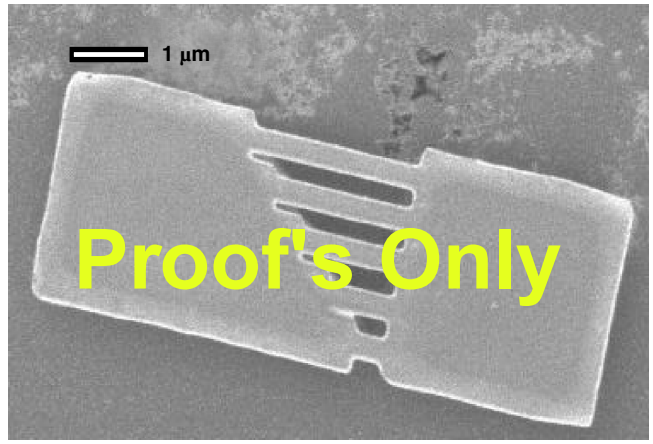

Figure 1. An ion micrograph of an array of nanobridges fabricated from a single-crystal silicon using a focused ion beam doping technique.

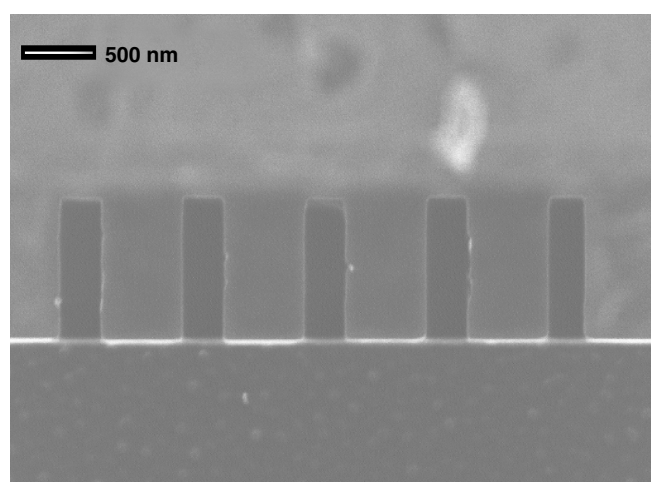

Figure 2. An ion micrograph of an array of nanocantilevers fabricated from commercially available microcantilevers using a focused ion beam.

cantilever and detection system is shown in Figure 3. The length of the cantilever was 4.5 μm and the thickness of the cantilever was 0.5 μm. This type of geometry allowed in-plane motion of the cantilever. The motion of the cantilever was in the plane of the image. The micrograph shows the thickness of the cantilever. Two electrodes (labeled as source and drain) were micromachined in such a way that the cantilever can oscillate between these two structures. The source and drain electrodes were equidistant from the cantilever beam. The separation distance between the cantilever and the source and drain was approximately 50 nm. All three components—cantilever (gate), source, and drain—were electrically isolated from each other. The nanocantilever was excited into resonance using an acoustic excitation source. The source and drain electrodes were electrically biased and the current flowing through the system was measured using a pico-ammeter. All measurements were performed under ambient conditions.

4.3. Nanocantilever Resonance Response Characterization

We studied the motion of the nanofabricated cantilevers using the experimental set-up described above [44]. When a bias voltage is applied between the source and drain electrodes, no electron current flowed through the system under d.c. voltage condition because of the air gap between the cantilever and the two electrodes. It is possible that when the system is biased with a d.c., the cantilever can bend due to applied electrostatic force. However, such cantilever bending due to electrostatic force was too small to cause the cantilever to bend enough and make contact with the electrodes. Also, since d.c. bias voltage is used, no displacement current flowed through the system. When the cantilever was excited into resonance (using an acoustic source), the oscillatory motion caused the cantilever to make electrical contact with the source and the drain electrode. Electronic charge was transferred to the electrically floating cantilever "gate" when the cantilever made contact with the source electrode. The electron charge on the cantilever was subsequently transferred to the drain electrode as the cantilever oscillated in the opposite direction and made contact with the drain electrode. As the cantilever made intermittent alternating contact with the source and drain electrodes, electrical charge was transferred from the source to the drain electrode causing a net electron current to flow through the system.

The applied bias voltage between the source and the drain electrode was 500 mV. When the cantilever was acoustically excited, the current through the circuit exhibited a peak at 5.2 MHz (see Fig. 4). At resonance, the acoustic frequency used for cantilever excitation matches with natural frequency of the cantilever. In Figure 4, we show the electron current through the system measured with a pico-ammeter as a function of the acoustic frequency that excited the cantilever into motion. From the data in Figure 4, it appears that at resonance the electron current increases to 7 pA against the noise floor of 1.7 pA. The mechanical Q-factor of the cantilever was calculated to be around 10 when the device was operated in air. The Q-factor can be increased by an order of magnitude by operating in a He gas environment; when the cantilever oscillates in a low viscosity medium such as He oscillation damping is reduced. At the resonance frequency, the measured electron current was approximately 7 pA.

The flow of electron current between the source and drain electrodes, facilitated by the cantilever motion, can be understood as follows. As the cantilever comes in contact with the energized source electrode, the cantilever will pick up charge q, either by electron tunneling or by physical contact. This charge will then be transferred to the drain electrode as the cantilever oscillates and makes contact with the drain electrode. The total current due to electron transfer

Figure 3. An ion micrograph of a nanocantilever with a readout system fabricated from a single-crystal silicon using an FIB. The cantilever "gate" was actuated acoustically and had a resonance frequency of 5.2 MHz.

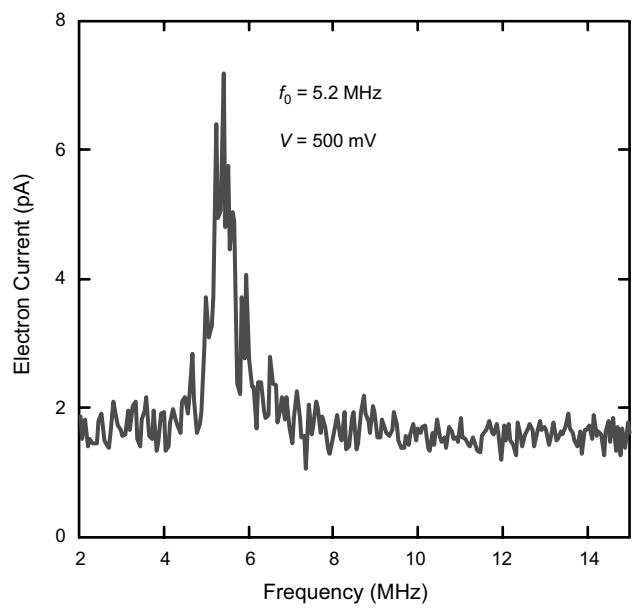

Figure 4. Electron current measured as a function of frequency. The nanocantilever gate was actuated acoustically around its first harmonic resonance and the effective electron transport was monitored for an applied bias of 500 mV.

can be expressed as

$$i = 2nef \tag{16}$$

where n is the number of charge quanta (electrons) transferred to the cantilever, e is the electronic charge, and f is the excitation frequency. From the data presented in Figure 4, we obtain a value of $n = 5$ at resonance and $n = 1$ at frequencies far away from resonance. These values correspond to 1.7 pA noise current and 7 pA current at resonance, respectively.

From the physical dimensions of the Si nanocantilever, a cantilever mass of 10–15 g can be calculated. If the resonance frequency can be measured with a resolution of 100 Hz, the minimum detection limit for adsorbed mass can be calculated as 10^{-19} g at a resonance frequency of 5.2 MHz. This detection limit is ample to detect changes in adsorbed mass due to a single biomolecule of a large protein or a DNA strand of 50 nm in length. The detection limit can be further improved by increasing the Q-factor of the cantilever. The Q-factor can be possibly amplified by a feedback system, which was demonstrated for optical signal transduction.

4.4. Femtogram Mass Sensitivity

Mass sensitivity of a few femtograms was demonstrated using small-size cantilevers in the air. The smaller cantilevers were fabricated from commercially available cantilevers (200 μm long, 50 μm wide, and 1.5 μm thick) and were coated with a 35-nm gold layer on one side to increase optical reflectivity and response to photothermal actuation [38]. An FIB milling instrument (FEI 200) was used to fabricate cantilevers that measured 2 to 6 μm long, 50 to 100 nm thick, and had resonance frequencies in the range of 1–6 MHz [38]. It was reported that all these fabricated resonators exhibited very similar normalized widths of the resonances in air, which was almost independent of the cantilever thicknesses and shapes. The explanation offered [38] was that for cantilevers in air, viscous damping by the medium is the predominant energy dissipation mechanism. Based on the width of the measured resonance curves, a Q-factor of 25 was estimated. At a lower air pressure, the Q-factor increased by at least five-fold. A very important conclusion that can be drawn from these observations is that minimization of intrinsic mechanical losses may not be practical in the case of nanomechanical mass-sensitive transducers operating in the air at room temperature and atmospheric pressure [38].

A rectangular, gold-coated silicon cantilever with a resonance frequency of 2.25 MHz with an approximate 2 μm width and 6 μm length was exposed to 11-mercaptoundecanoic acid vapor. Upon exposure of the cantilever to 11-mercaptoundecanoic acid vapors, the resonance frequency was found to decrease, which was attributed to chemisorption of the analyte molecules onto the gold-coated surface of the cantilever. The measured frequency shift of 2 KHz was found to correspond to an added mass of 5.5×10^{-15} g, a value that is close to a 50% coverage of a monolayer of 11-mercaptoundecanoic with a total mass of 6×10^{-15} g over the area of the cantilever which is 12 μm^2.

4.5. Controlling *Q*-Factor of a Cantilever

The Q-factor of a cantilever, defined as the ratio of resonance frequency to FWHM of a resonance curve, determines the efficiency of oscillations. The Q of a microcantilever vibrating in air is approximately the 100–30 range, while under liquid Q drops to an extremely small value of approximately 1. The resolution of the resonance frequency measurement increases with Q. Therefore, techniques to improve the Q-factor of vibrating cantilevers will have important implications in imaging and sensor applications. Recently, it has been demonstrated that the Q of a cantilever vibration can be manipulated using a feedback technique [22, 46]. It is shown that the Q can be increased by a factor 10–1000 using feedback. Even Brownian motion (thermal motion) of a cantilever can be amplified.

As pointed out earlier, a low Q-factor leads to a lower resolution in resonance frequency detection and thus a low sensitivity in mass detection. When the cantilever sensor is operated in a medium, the damping decreases the Q-factor leading to lower sensitivity. Therefore, despite its suitability for liquid operations resonance, frequency-based, cantilever sensors have not attracted much attention as sensitive biological and chemical sensors. The Q-factor of a cantilever can be increased by utilizing a feedback technique. For an optical beam deflection technique, the feedback can be accomplished by feeding back the output of the PSD to a piezoelectric cantilever holder. A phase shifter and a gain controller placed between the PSD and piezoelectric holder determines the feedback condition. By adjusting the phase shift and gain, the Q-factor can be manipulated in a controlled fashion.

The governing equation of motion for a feedback-driven cantilever, modeled as a damped harmonic oscillator, is

$$m_{eff}\frac{d^2z}{dt^2} + \gamma\frac{dz}{dt} + kz = Ge^{i\phi}z(t) \tag{17}$$

where, m_{eff} is the effective mass of the cantilever, γ is the resistance or damping force on the cantilever, k is the spring constant, G is the gain of the feedback amplifier, ϕ is the phase shift added by the phase shifter, and z is the vertical displacement of the cantilever. Thus the system can be thought of as a harmonic oscillator with an effective spring constant $k_{eff} = (k - Ge^{i\phi})$. The general form of the solution for $z(t)$ can be written as

$$z(t) = (C_1 \cos\omega^* t + C_2 \sin\omega^* t)e^{-\frac{\gamma t}{2m_{eff}}};$$
$$\text{where } \omega^* = \sqrt{\frac{k_{eff}}{m_{eff}} - \frac{\gamma^2}{4m_{eff}^2}} \tag{18}$$

The gain of the feedback amplifier (G) and phase shift (ϕ) was critical in tuning the feedback signal to achieve resonance and amplification. The magnitude of the gain and phase shift was a function of the physical dimensions and material properties of the cantilever. We have shown that the Q-factor of a silicon-nitride cantilever oscillating under a solution can be varied. In air, we were able to increase the Q from 20 to 3000 for silicon-nitride cantilevers resonating by Brownian motion. The smaller FWHM achieved with the feedback allows frequency measurements at a

smaller linewidth, improving the minimum detectable frequency shift. Similar Q-factor enhancement can be achieved for other signal transduction methods [7, 22, 46].

5. FUTURE OUTLOOK

As the technology to fabricate nanosize mechanical structures further develops, we envision a plethora of new application where these systems can play an important role. As the frequency of these devices approaches or even exceeds GHz nanomechanical devices will be in the same time and frequency domain reserved now only for electronic devices.

One very important issue that need to be addressed is the efficient readout of nanocantilevers not only because of the small size but also because of the readout of large arrays. Compared to presently used signal transduction methods, electron transfer using a cantilever system is ideally suited for NEMS nanocantilevers. Conventional techniques of measuring the resonance frequency, such as optical beam deflection, fall short when applied to micromachined nanocantilevers. For example, in optical beam deflection, the cantilever motion is measured by reflecting a laser diode off the free end of a cantilever into a position-sensitive detector. The shortcomings of optical techniques are simply due to the lack of a sufficient reflected (or scattered) optical signal from the cantilever beam. Optical beam deflection is extremely sensitive when used for cantilevers that are 5 μm to a few hundreds of micrometers long while the electron transfer signal transduction is extremely sensitive for cantilevers that are a few hundred nanometers to a few microns in length.

The applicability of electron transfer signal transduction for aqueous environments is extremely challenging. Presence of electro active ions in the water can cause a large Faraday leakage current that can overwhelm electron transfer signal. The leakage current, however, can be significantly reduced using proper insulation, reduced bias voltage, and a reduced number of charge carriers in the solution. However, this technique may be applicable for biosensors that can be operated in humid atmosphere.

GLOSSARY

REFERENCES

1. T. Thundat, R. J. Warmack, Chen, and D. P. Allison, *Appl. Phys. Lett.* 64, 2894 (1994).
2. T. Thundat, G. Y. Chen, R. J. Warmack, D. P. Allison, and E. A. Wachter, *Anal. Chem.* 67, 519 (1995).
3. T. Thundat, E. A. Wachter, S. L. Sharp, and R. J. Warmack, *Appl. Phys. Lett.* 66 (1995).
4. P. G. Datskos, C. M. Egert, and I. Sauers, *Sensors and Actuators B* 61, 75 (2000).
5. J. K. Gimzewski, C. Gerber, E. Meyer, and R. R. Schlittler, *Chem. Phys. Lett.* 217, 589 (1994).
6. R. Berger, C. Gerber, H. P. Lang, and J. K. Gimzewski, *Microelectronic Engineering* 35, 373 (1997).
7. G. Abadal, Z. J. Davis, B. Helbo, X. Borris, R. Ruiz, A. Boisen, F. Campabadal, J. Esteve, E. Figueras, F. Perez-Murano, and N. Barniol, *Nanotechnology* 12, 100 (2001).
8. T. Thundat, P. I. Oden, P. G. Datskos, G. Y. Chen, and R. J. Warmack, in "The 16th Warner Brandt Workshop on Charged Particle Penetration Phenomena." Oak Ridge, TN, 1996.
9. N. V. Lavrik, C. A. Tipple, M. J. Sepaniak, and P. G. Datskos, *Biomedical Microdevices* 3, 33 (2001).
10. N. V. Lavrik, C. A. Tipple, M. J. Sepaniak, and P. G. Datskos, *Proc. SPIE* 4560, 152 (2001).
11. N. V. Lavrik, C. A. Tipple, M. J. Sepaniak, and P. G. Datskos, *Chem. Phys. Lett.* 336, 371 (2001).
12. H. P. Lang, R. Berger, F. Battistion, J. P. Ramseyer, E. Meyer, C. Andreoli, J. Brugger, P. Vettiger, M. Despont, T. Mezzacasa, L. Scandella, H.-J. Guntherodt, C. Gerber, and J. K. Gimzewski, *Appl. Phys. A* 66, S61 (1998).
13. H. P. Lang, M. K. Baller, R. Berger, C. Gerber, J. K. Gimzewski, F. M. Battison, P. Fornaro, J. P. Ramseyer, E. Meyer, and H. J. Gÿntherodt, *Anal. Chim. Acta* 393, 59 (1999).
14. H. P. Lang, R. Berger, C. Andreoli, J. Brugger, M. Despont, P. Vettiger, C. Gerber, J. K. Gimzewski, J. P. Ramseyer, E. Meyer, and H.-J. Güntherodt, *Appl. Phys. Lett.* 72, 383 (1998).
15. P. G. Datskos, M. J. Sepaniak, C. A. Tipple, and N. Lavrik, *Sensors and Actuators B-Chemical* 76, 393 (2001).
16. P. G. Datskos, S. Rajic, M. J. Sepaniak, N. Lavrik, C. A. Tipple, L. R. Senesac, and I. Datskou, *J. Vac. Sci. Tech. B* 19, 1173 (2001).
17. J. C. L. Britton, R. L. Jones, P. I. Oden, Z. Hu, R. J. Warmack, S. F. Smith, W. L. Bryan, and J. M. Rochelle, *Ultramicroscopy* 82, 17 (2000).
18. R. Berger, E. Delamarche, H. P. Lang, C. Gerber, J. K. Gimzewski, E. Meyer, and H.-J. Güntherodt, *Science* 276, 2021 (1997).
19. D. Sarid, "Scanning Force Microscopy with Applications to Electric, Magnetic, and Atomic Forces." Oxford University Press, New York, 1991.
20. G. Y. Chen, T. Thundat, E. A. Wachter, and R. J. Warmack, *J. Appl. Phys.* 77, 3618 (1995).
21. T. R. Albrecht, P. Grutter, D. Horne, and D. Rugar, *J. Appl. Phys.* 69, 668 (1991).
22. A. Mehta, S. Cherian, D. Hedden, and T. Thundat, *Appl. Phys. Lett.* 78, 1637 (2001).
23. E. A. Wachter, T. Thundat, P. G. Datskos, P. I. Oden, R. J. Warmack, and S. L. Sharp, *Rev. Sci. Instrum.* 67 (1996).
24. M. Tortonese, H. Yamada, R. C. Barrett, and C. F. Quate, in "The Proceedings of Transducers '91." *IEEE,* Pennington, NJ, 1991.
25. M. Tortonese, R. C. Barrett, and C. F. Quate, *Appl. Phys. Lett.* 62, 834 (1996).
26. J. A. Harley and T. W. Kenny, *J. Microelectromechanical Systems* 9, 226 (2000).
27. P. I. Oden, E. A. Wachter, P. G. Datskos, T. Thundat, and R. J. Warmack, *Infrared Technology and Applications XXII,* SPIE 2744, 345 (1996).
28. D. L. DeVoe and A. P. Pisano, *J. Microelectromechanical Systems* 6, 266 (1997).
29. S. Zurn, M. Hseih, G. Smith, D. Markus, M. Zang, G. Hughes, Y. Nam, M. Arik, and D. Polla, *Smart Materials and Structures* 10, 252 (2001).
30. Q. M. Wang and L. E. Cross, *Ferroelectrics* 215, 187 (1998).
31. R. Amantea, C. M. Knoedler, F. P. Pantuso, V. K. Patel, D. J. Sauer, and J. R. Tower, in "SPIE," Vol. 3061, p. 210. Orlando, FL, 1997.
32. G. G. Stoney, *Proc. Royal Soc. London* 82, 172 (1909).
33. R. Shuttleworth, *Proc. Phys. Soc. London* 63A, 444 (1950).
34. Y. T. Yang, K. L. Ekinci, X. M. H. Huang, L. M. Schiavone, and M. L. Roukes, *Appl. Phys. Lett.* 78, 162 (2001).
35. D. W. Carr, L. Sekaric, and H. G. Craighead, *J. Vac. Sci. Tech. B* 16, 3821 (1998).
36. A. Olkhovets, S. Evoy, D. W. Carr, J. M. Parpia, and H. G. Craighead, *J. Vac. Sci. Tech.* B18, 3549 (2000).

37. Z. J. Davis, G. Abadal, O. Kuhn, O. Hansen, F. Grey, and A. Boisen, *J. Vac. Sci. Tech. B* 18 (2000).
38. N. V. Lavrik and P. G. Datskos, *Appl. Phys. Lett.* 82, 2697 (2003).
39. U. Drodofsky, M. Drewsen, T. Pfau, S. Nowack, and J. Mlynek, *Microelectronic Engineering* 30, 383 (1996).
40. H. Kawakatsu, H. Toshiyoshi, D. Saya, K. Fukushima, and H. Fujita, *Appl. Surf. Sci.* 57, 320 (2000).
41. J. Brugger, G. Beljakovic, M. Despont, N. F. deRooij, and P. Vettiger, *Microelectronic Engineering* 35, 401 (1997).
42. M. T. Tuominen, R. V. Krotkov, and M. L. Breuer, *Phys. Rev. Lett.* 83, 3025 (1999).
43. J. Xu and A. J. Steckl, *Appl. Phys. Lett.* 65, 2081 (1994).
44. P. G. Datskos and T. Thundat, *J. Nanosci. Nanotech.* 2, 369 (2001).
45. A. J. Steckl, H. C. Mogul, and S. Mogren, *Appl. Phys. Lett.* 60, 1833 (1992).
46. J. Tamayo, A. D. L. Humphris, and M. J. Miles, *Appl. Phys. Lett.* 77, 582 (2000).